

# Transient fields radiated by curved surfaces—Application to focusing

Daniel Guyomar and John Powers

Department of Electrical and Computer Engineering, Naval Postgraduate School, Monterey, California 93943

(Received 8 April 1984; accepted for publication 27 June 1984)

A theoretical model is presented for computing the transient radiated field (potential or pressure) resulting from a curved surface having an arbitrary velocity distribution. The method is a generalization of the angular spectrum theory giving the time impulse response for a given shaped surface. The technique leads to a systems theory interpretation of the radiation and diffraction effects. General expressions for arbitrary surfaces are given but important simplifications occur for radially symmetric geometries. For this case, simple expressions for the wave location may be obtained without requiring solution of the wave. Numerical simulations for common focused waves are given using computationally efficient FFT algorithms.

PACS numbers: 43.20.Px, 43.20.Rz, 43.20.Bi

## LIST OF SYMBOLS

$x, y, z, r$	space coordinates
$\phi(x, y, z, t)$	velocity potential at position $(x, y, z)$ at time, $t$
$\gamma(t)$	temporal portion of velocity excitation
$s(x, y)$	spatial portion of velocity excitation
$d(x, y)$	relative delay distance over aperture surface
$\Delta(x, y)$	relative temporal delay over aperture surface
$f$	focal length of acoustic lens
$L_1, L_2$	propagation distance in lens and medium
$c_1, c_2$	sound velocity in lens and medium
$f(x, y)$	lens thickness profile
$x_m, y_m$	location of maximum of $f(x, y)$

$f_x, f_y, \rho$	spatial frequencies (Cartesian and radial)
$F_{xy} [ ], F_{xy}^{-1} [ ]$	direct and inverse 2-D spatial Fourier transform operators
$B [ ], B^{-1} [ ]$	direct and inverse Hankel transform operators
$G(f_x, f_y, z, t)$	spatial Fourier transform of $\phi(x, y, z, t)$ for impulse time excitation
$x_i^*, r_i^*$	$i$ th zero of $d(x, y) - ct = 0$ or $d(r) - ct = 0$
$A$	transducer size (half-width or radius)
$N$	total number of zeros of $d(x, y) - ct = 0$ or $d(r) - ct = 0$
$\min [ ]$	operator that returns the minimum of a function
$\max [ ]$	operator that returns the maximum of a function

## INTRODUCTION

The description of the field produced by a source is very important due to its use in acoustic techniques that image or scatter the wave. Depending on the application, the wave fronts may be planar or curved. For nonplanar wave fronts, the curvature is usually either concave (focused field) or convex (diffused field). Techniques for generating curved wave fronts include curved transducers, acoustic lenses, and traveling wave excitation (or, equivalently, phased arrays).

Transient solutions for planar waves and sources have been investigated in recent years<sup>1-10</sup> and different techniques are now available for computing the field of these sources. The transient solution from a curved source has received less attention. A closed form solution for the special case of a concave spherical radiator has been given in Refs. 11 and 12. Other solutions appear in Refs. 13-15. Curved transducers are different to work with and represent a complex transduction of the electrical signal into an acoustic wave. Many common sources will cover a planar transducer with a lens or will

use a time-dependent electric excitation applied to segmented transducer arrays to simplify the excitation. The resulting acoustic field, however, remains identical (or as close as possible) to the one generated by a curved transducer. Our aim is to present a theoretical method for computing the expected transient acoustic field of a baffled radiator with an arbitrary velocity distribution and an arbitrary delay on its surface. The curved wave fronts can be produced by a lens, an array, or a slightly curved transducer. For the lens and curved transducer cases, the restriction to slight curvature implies that the waves do not reflect off of surfaces on the opposite side of the transducer. The propagation medium is assumed to be homogeneous and isotropic in this technique.

## I. BASIC THEORY

### A. General case

For a planar rigid-baffled transducer, it is known from diffraction theory that the velocity potential is related to the source velocity distribution by

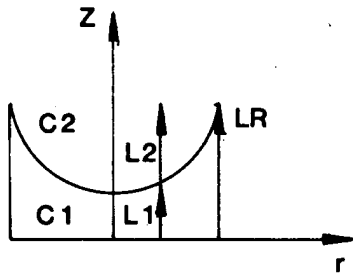


FIG. 1. Geometry for propagation through acoustic lens element.

$$\phi(x, y, z, t) = \gamma(t) s(x, y) \underset{xyr}{***} [\delta(ct - R)/R], \quad (1)$$

where  $s(x, y)$  and  $\gamma(t)$  represent the space and time-varying parts of the known velocity disturbance at the input plane, \* indicates convolution performed over the indicated variable, and

$$R = (x^2 + y^2 + z^2)^{1/2}. \quad (2)$$

The expression  $\delta(ct - R)/R$  in Eq. (1) is the Green's function for free-space propagation.

The curvature of the wave can be modeled by a spatially variable delay from a plane wave. For a lens, this delay results from the velocity difference between the lens material and the propagation medium. For a separable velocity disturbance the field can be written as

$$\begin{aligned} \phi(x, y, z, t) \\ = \gamma(t) \underset{t}{*} s(x, y) \delta[ct - d(x, y)] \underset{xyr}{***} [\delta(ct - R)/R], \end{aligned} \quad (3)$$

where  $d(x, y)$  is the thickness of the equivalent lens causing the delay. (Expressions for this time delay for various emitters are given in Appendix B.)

As an example, if we consider a spherical lens (Fig. 1), the time delay over the surface at the radial position  $r$ , relative to the time delay encountered at the edge of a lens, is

$$\Delta(r) = \left[ \frac{L_1}{c_1} + \frac{L_2}{c_2} \right] - \frac{L_R}{c_1}, \quad (4)$$

where the term in brackets is the delay encountered from the portion of the wave traveling through a distance  $L_2$  in the propagation medium and a distance  $L_1$  in the lens. The last term in the expression is the delay of the wave traveling in the edge of the lens. The velocities of the medium and the lens material are  $c_2$  and  $c_1$ , respectively. After some algebra, Eq. (4) becomes

$$\Delta(r) = [(c_1 - c_2)(L_R - L_1)]/c_1 c_2. \quad (5)$$

Because of this delay, the wave front will be displaced (i.e., curved) by a distance  $d(r)$ ,

$$d(r) = c_2 \Delta(r). \quad (6)$$

For the general case, if we consider a lens thickness profile of the form  $f(x, y)$ , with a maximum thickness located at  $(x_m, y_m)$ , then the time delay, relative to the delay encountered at the thickest part, will be

$$\Delta(x, y) = [(c_1 - c_2)/c_1 c_2] [f(x_m, y_m) - f(x, y)] \quad (7)$$

and the relative wave displacement will be

$$d(x, y) = c_2 \Delta(x, y). \quad (8)$$

Although this discussion has been in terms of an acoustic lens modifying a plane wave, it should be noted that the same

ideas can be applied to any curved wave front, regardless of the techniques used for its production. All one needs for the propagation technique to be described is a description of the wave front in terms of either its relative displacement,  $d(x, y)$ , or its time delay,  $\Delta(x, y)$ .

Because of the symmetry of the  $\delta$  function in Eq. (3) and for efficiency of computation, it is convenient to use the  $(f_x, f_y, z, t)$  space.<sup>10</sup> Propagation in this space corresponds to a time generalization of the angular spectrum theory, leading to a linear systems interpretation of the transient diffraction. The diffraction is equivalent to a time varying spatial filter acting on the source spatial spectrum.<sup>10</sup>

Recall that

$$\delta[f(x)] = \sum_{i=1}^N \delta(x - x_i) \left/ \left| \frac{df}{dx} \right|_{x=x_i} \right., \quad (9)$$

where  $x_i$  are the zeros of  $f(x)$ . Using this expansion we have an expression for the Green's function portion of Eq. (1),

$$\frac{\delta(ct - R)}{R} = \frac{\delta[r - (c^2 t^2 - z^2)^{1/2}]}{R [(c^2 t^2 - z^2)^{1/2}/ct]}, \quad (10)$$

where  $r = (x^2 + y^2)^{1/2}$ . Taking the Fourier-Bessel transform (i.e., the Fourier transform of a radially symmetric field) will lead to an expression for the transform of the Green's function given by

$$\begin{aligned} B \left[ \frac{\delta(ct - R)}{R} \right] &= B \left[ \frac{\delta[r - (c^2 t^2 - z^2)^{1/2}]}{R [(c^2 t^2 - z^2)^{1/2}/ct]} \right] \\ &= J_0[\rho(c^2 t^2 - z^2)^{1/2}] H(ct - z), \end{aligned} \quad (11)$$

where  $B[\cdot]$  is the Fourier-Bessel (or Hankel) transform operator and  $\rho = (f_x^2 + f_y^2)^{1/2}$ . The zero-order Bessel function  $J_0$  is the transfer function of the diffraction process. It shows how the high spatial frequencies are reduced at any  $z$  plane as time increases. The transform of the potential due to an impulse of the form,  $\delta[ct - d(x, y)]$ , can be written from Eqs. (3) and (12) as

$$\begin{aligned} G(f_x, f_y, z, t) &= F_{xy} [s(x, y) \delta(ct - d(x, y))] \\ &\quad \times \underset{t}{*} J_0[\rho(c^2 t^2 - z^2)^{1/2}] H(ct - z), \end{aligned} \quad (13)$$

where  $F_{xy}[\cdot]$  is the two-dimensional spatial transform operator. Extending Eq. (9) to the two-dimensional space, we have

$$\begin{aligned} F_{xy} [s(x, y) \delta(ct - d(x, y))] \\ = \int_0^\infty \sum_{i=1}^N \left( s[x_i^*(y), y] \left/ \left| \frac{\partial d[x_i^*(y), y]}{\partial x} \right| \right) \right. \\ \quad \times \exp\{-i[f_x x_i^*(y) + f_y y]\} dy \\ = F_y \left[ \sum_{i=1}^N \left( s[x_i^*(y), y] \left/ \left| \frac{\partial d[x_i^*(y), y]}{\partial x} \right| \right) \right. \right. \\ \quad \left. \left. \times \exp[-if_x x_i^*(y)] \right], \end{aligned} \quad (14)$$

where  $x_i^*(y)$  represents the values of  $x$  for which  $d(x, y) - ct = 0$  for fixed  $y$ . Here,  $N$  is the number of zeros. [Appendix B displays expressions for the relative displacement  $d(x, y)$ , the zeros of  $d(x, y) - ct$ , and the derivative in the denominator of Eq. (15) for various wave-front configurations.] It is worth noting that Eq. (13) is the time-depen-

dent spectrum of a line source affected by a varying amplitude. This line source is determined by the intersection of the  $d(x, y)$  surface with a plane parallel to the  $(x, y, 0)$  plane at a location  $z = ct$ . As time increases, the size (and shape) will change. Since the two-dimensional transform is now along a line, the two-dimensional Fourier transform becomes a one-dimensional transform. Equations (14) and (15) remain the same for either a convex or a concave surface delay  $d(x, y)$ . The formulation of Eqs. (13) and (15) is valid, generally, for the emission from any curved surface as well as transmission through a thin lens.

The field,  $g(x, y, z, t)$ , is obtained by inverse transforming Eq. (13) to give

$$g(x, y, z, t) = F_{xy}^{-1} \left[ F_y \left[ \sum_{i=1}^N \left( s[x_i^*(y), y] \left/ \left| \frac{\partial d[x_i^*(y), y]}{\partial x} \right| \right) \right] \right] \times \exp \left[ -if_x x_i^*(y) \right] J_0 \left[ \rho(c^2 t^2 - z^2)^{1/2} \right]. \quad (16)$$

This equation gives the output field for an arbitrary shape of surface velocity when excited by an impulse in time. The curvature of the field is contained in the expression for  $x_i^*$ .

For an arbitrary time function we must convolve (over time) the result of Eq. (16) with the time dependent excitation as in Eq. (1). In most sources, the delay function,  $d(x, y)$ , is separable in  $x$  and  $y$  dependence (or dependent on only one variable). The functions of Appendix B illustrate this point. These conditions make the  $F_y[\cdot]$  operation easier to compute. Usually a time convolution and a two-dimensional Fourier transform over the calculated frequencies will be the only computations required. With the use of FFT routines the computation is very efficient and rapid, allowing the velocity potential to be calculated over the entire  $xy$  plane.

Equation (16) represents the velocity potential for an impulse temporal excitation when the velocity over the emitting surface is known. From the potential, one obtains the pressure,  $P(x, y, z, t)$ , from the relation

$$P(x, y, z, t) = \rho_0 \frac{\partial \phi(x, y, z, t)}{\partial t}, \quad (17)$$

where  $\rho_0$  is the density of the medium. From Eq. (16) we find an expression for the pressure with an impulse time excitation as

$$P(x, y, z, t) = \rho_0 F_{xy}^{-1} \left[ F_y \left[ \sum_{i=1}^N \left( s[x_i^*(y), y] \left/ \left| \frac{\partial d[x_i^*(y), y]}{\partial x} \right| \right) \right] \right] \times \exp \left[ -if_x x_i^*(y) \right] \frac{\rho c^2 t}{(c^2 t^2 - z^2)^{1/2}} \times J_1 \left[ \rho(c^2 t^2 - z^2)^{1/2} \right]. \quad (18)$$

Hence either the potential or pressure are easily and efficiently computed with this technique. It is worth noting that as  $ct$  approaches  $z$ , the function  $J_1[\rho(c^2 t^2 - z^2)^{1/2}]/(c^2 t^2 - z^2)^{1/2}$  approaches a Dirac delta function.

## B. Axisymmetric delay and displacement

A large fraction of transducers are of axisymmetric geometry, therefore, the delay and the displacement of the transducer are radial functions. For such symmetry the one-dimensional Hankel transform can be substituted for the two-dimensional spatial transform. Then Eqs. (13) and (16) can be written as

$$\phi(\rho, z, t) = B(s(r)\delta[ct - d(r)]) \times J_0[\rho(c^2 t^2 - z^2)^{1/2}] H(ct - z) \quad (19)$$

and

$$\phi(r, z, t) = B^{-1} \left[ \sum_{i=1}^N \left( s(r_i^*) J_0(\rho r_i^*) r_i^* \left/ \left| \frac{\partial d(r)}{\partial r} \right|_{r=r_i^*} \right) \right] \times J_0[\rho(c^2 t^2 - z^2)^{1/2}], \quad (20)$$

respectively, where  $B[\cdot]$  is the Hankel transform operator and  $r_i^*$  denotes the zeros of  $ct - d(r)$ .

The terms of the summation represent the angular spectrum of a circular line source weighted by the function,  $s(r_i^*)$ . The radius of such a line varies with time according to the delay law since  $r_i^*$  is a function of time. The resulting field is just the summation of these line-generated waves plus the diffraction field that has been generated by the previous line excitations. Once again, the field computation requires only one convolution for the computed frequencies and a Hankel transform.<sup>16</sup>

A simpler version of Eq. (20) may be found by inverting the integration order (see Appendix A). This formulation imposes conditions on the radial distance and consequently defines the domain where the waves will propagate.

Again, field solutions for an arbitrary time excitation may be obtained by convolution of the impulse response with the time excitation.

## II. NUMERICAL SIMULATIONS

Once the geometry of the transducer is known, an elementary calculation leads to the relative displacement of the wave,  $d(x, y)$ . Then the  $N$  zeros of  $ct - d(x, y)$  are calculated. These are  $x_i^*(y)$  or  $r_i^*$ . These solutions are then used in Eqs. (16) or (20). Standard FFT algorithms perform the transforms. The convolution is done numerically for each spatial frequency. The results of the convolution are then inversely transformed to give the resulting values of the field. (It is worth noting that the calculation of the convolution uses the same products required for the transform, thereby reducing the computational complexity of the required operations.)

If the displacement,  $d(x, y)$ , is a monotonic function, then the intersection with the plane,  $z = ct$ , will reduce to a closed line and the summation in the equations will reduce to a single term. This is usually the case for a focused wave.

The main features of the method are that the use of the FFT allows efficient calculations with low computer times and that the method does not require any specific sampling period in time. Arbitrary regions of time, therefore, can be investigated with smaller increments of time than other regions that require less temporal resolution.

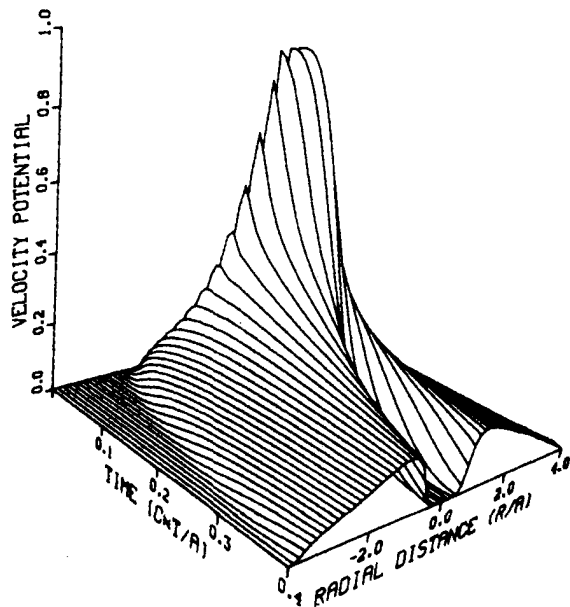


FIG. 2. Spherical concave wave with a circular cross section (impulse excitation,  $A = 2.0$  cm,  $f = 10$  cm,  $z = 5$  cm).

The following simulations have been investigated using this technique:

- (1) a circular emitter with a spherical shaped concave delay,
- (2) a circular emitter with a conical concave shaped delay,
- (3) a circular emitter with a parabolic concave shaped delay,
- (4) a circular emitter with a spherical convex shaped delay, and
- (5) a square emitter with a cylindrical delay over its surface.

The corresponding delays for each of these shapes is given in Appendix B.

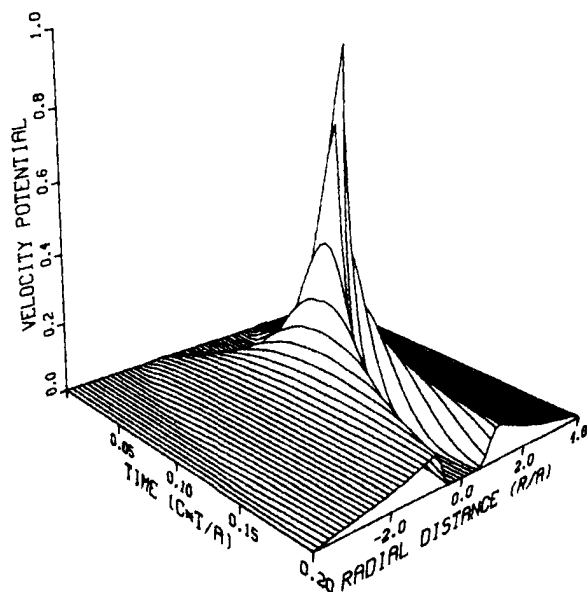


FIG. 3. Spherical concave wave with a circular cross section (impulse excitation,  $A = 2.0$  cm,  $f = 10$  cm,  $z = 10$  cm).

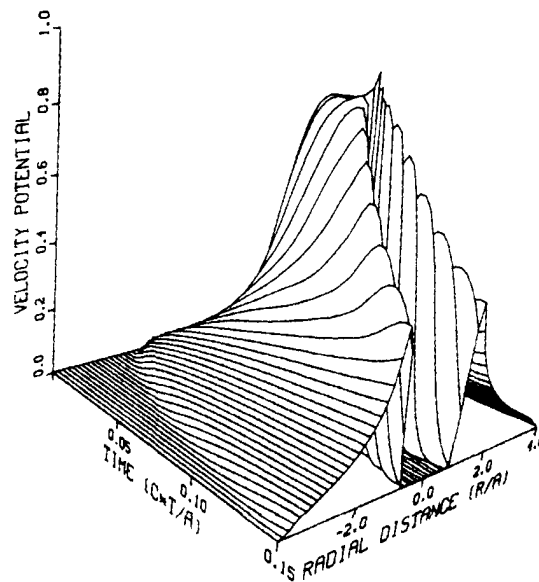


FIG. 4. Spherical concave wave with a circular cross section (impulse excitation,  $A = 2.0$  cm,  $f = 10$  cm,  $z = 20$  cm).

The computations were done on a grid of  $64 \times 64$  spatial sample points and 50 time samples. The plots show one spatial dimension versus time for a median through the center of the transducer. The complete three-dimensional calculation consumes approximately 80 s of CPU computer time on an IBM 3033 mainframe computer. For convenience the plots have been normalized to a maximum value of one. The time axis as well as the width axis are expressed in terms of one characteristic size  $A$  of the transducer (either half-width or radius, as appropriate). The time axis has a zero value at the time when the first wave reaches the observation line. For spherical, conical, and parabolic delays the field is presented at positions located at distances of  $f/2$ ,  $f$ , and  $2f$  from the emitter, where  $f$  is the focal length of the lens (assumed 10 cm in all of the simulations). The transducer radius  $A$  is as-

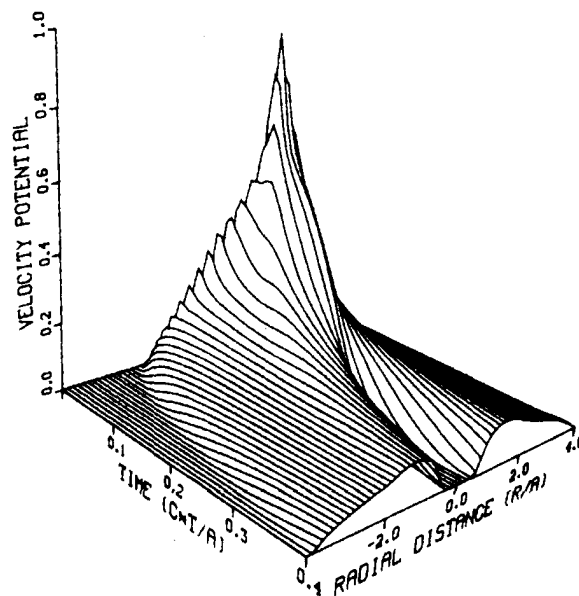


FIG. 5. Conical concave wave with a circular cross section (impulse excitation,  $A = 2.0$  cm,  $f = 10$  cm,  $z = 5$  cm).

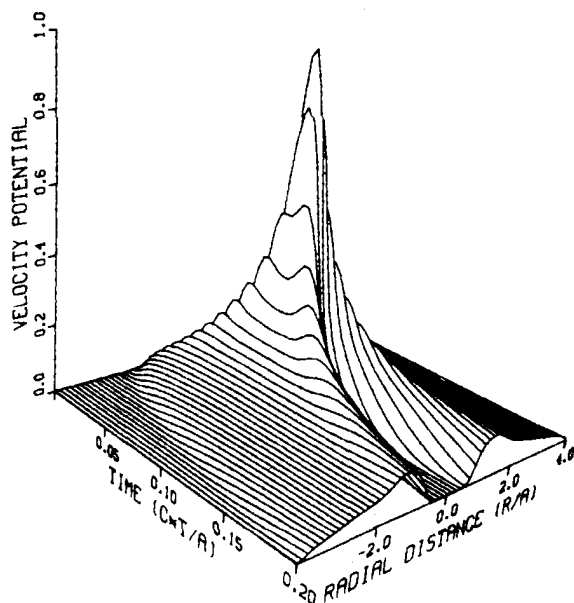


FIG. 6. Conical concave wave with a circular cross section (impulse excitation,  $A = 2.0$  cm,  $f = 10$  cm,  $z = 10$  cm).

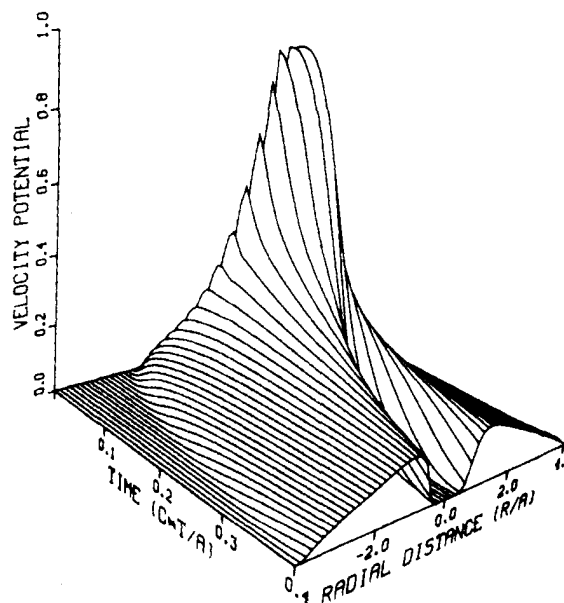


FIG. 8. Parabolic concave wave with a circular cross section (impulse excitation,  $A = 2.0$  cm,  $f = 10$  cm,  $z = 5$  cm).

sumed to be 2.0 cm and the excitation is an impulse (except for Figs. 16 and 17 as will be discussed).

Figures 2–4 show the diffraction pattern from a circular wave front with a spherical concave surface. While the solution of Eq. (20) is obtained in a plane parallel to the excited surface the plots have been shown with time as the variable to allow comparison with existing solutions.<sup>11,12</sup> The results fit the closed form solution of Refs. 11 and 12 very well. Symmetry is observed when the field is observed at the focal distance (Fig. 3). From a Dirac function on the time axis, the field becomes smoother as the radial distance increases. In front of the focal plane (Fig. 2) the field reaches a maximum early on the time axis and then decreases in value with increasing time. When the field is observed behind the focal

plane (Fig. 4), the field rises slowly to a maximum then abruptly falls to zero value, resulting in a so-called “time inversion” from the case located in the front focal plane. Along a line of constant time the field is relatively narrow in space indicating that the wave packet stays relatively close together for this curvature.

Figures 5–7 represent a wave front with a conical concave surface. The field evolves along the propagation axis but keeps the same features both in front of and behind the focal plane. As with the spherical transducer, there is a “time inversion” in the wave between the waves before and after the focal plane. In front of the focal plane the maximum is reached shortly after the first waves reach the observation plane. The maximum occurs sooner after the first waves

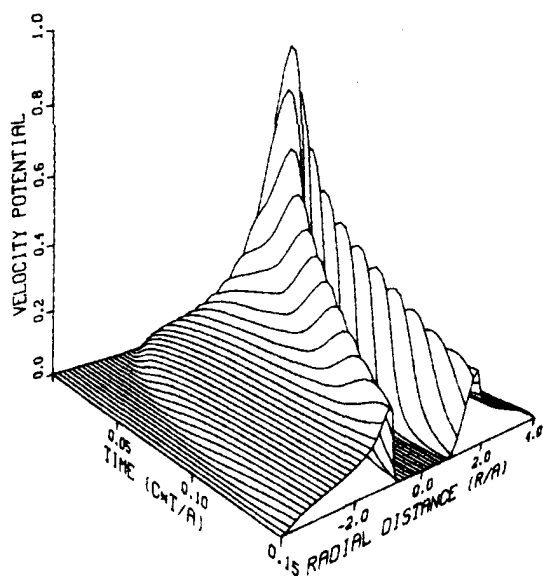


FIG. 7. Conical concave wave with a circular cross section (impulse excitation,  $A = 2.0$  cm,  $f = 10$  cm,  $z = 20$  cm).

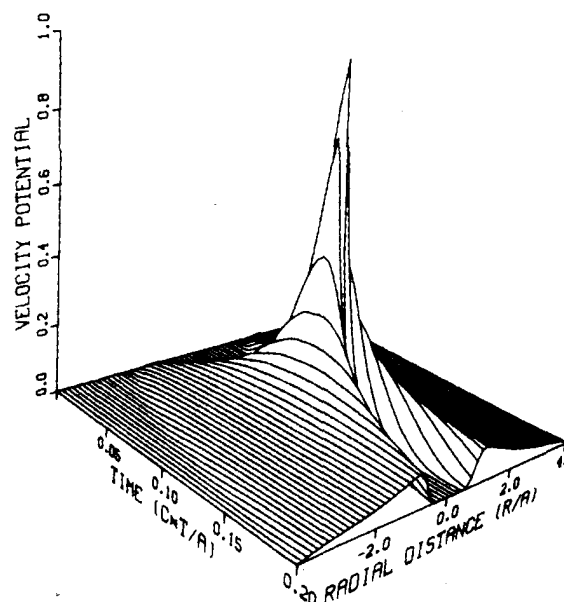


FIG. 9. Parabolic concave wave with a circular cross section (impulse excitation,  $A = 2.0$  cm,  $f = 10$  cm,  $z = 10$  cm).

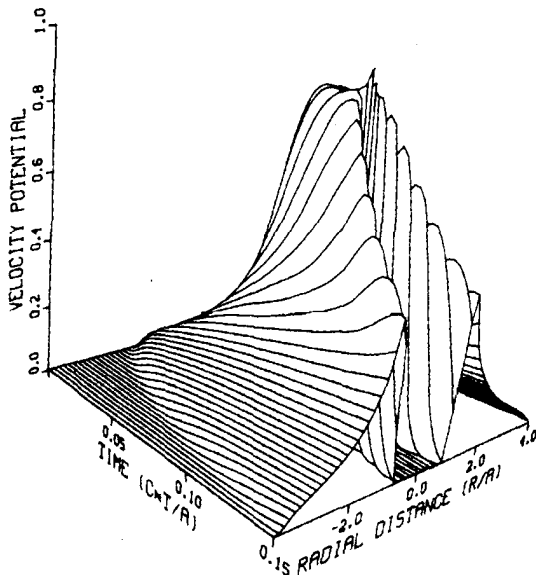


FIG. 10. Parabolic concave wave with a circular cross section (impulse excitation,  $A = 2.0$  cm,  $f = 10$  cm,  $z = 20$  cm).

have reached the observation plane than in the case of a spherical wave front. This result is in good agreement with Ref. 17. Another characteristic is that the wave stays concentrated around the axis for all values of distance, resulting in large depth of focus for this wave.

For a parabolic shaped wave (Figs. 8–10), the diffraction pattern has a shape very similar to that of the spherical wave, as might be expected since the fields are quite similar. The effects of the differences would be expected only at very large propagation distances or for very short focal lengths.

Figure 11 represents the radiation pattern of a convex spherical wave in front of the back focal plane. This lens tends to diverge the wave as expected.

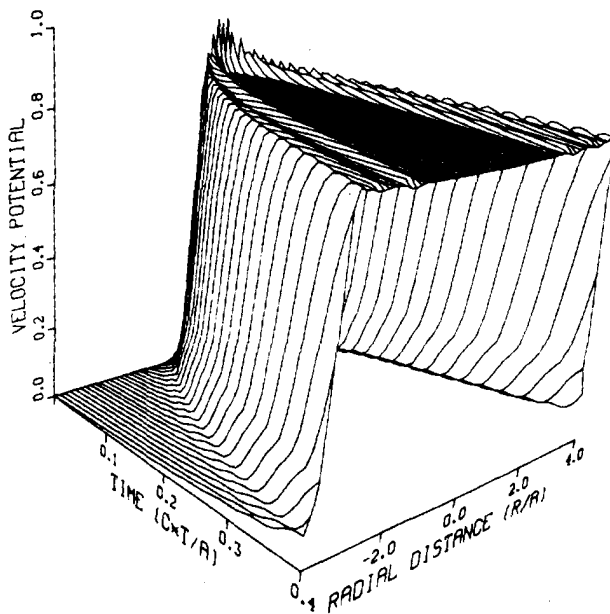


FIG. 11. Spherical convex wave with a circular cross section (impulse excitation,  $A = 2.0$  cm,  $f = 10$  cm,  $z = 5$  cm).

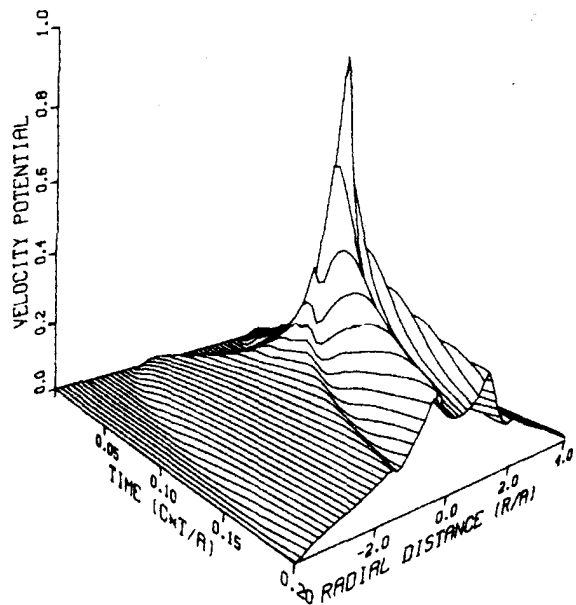


FIG. 12. Cylindrical concave wave over a square piston (impulse excitation,  $A = 2.0$  cm,  $f = 10$  cm,  $z = 5$  cm).

In Fig. 12 the field for a square transducer with a cylindrical lens is presented. The field is observed along a median plane oriented perpendicular to the cylindrical axis. For small values of time, the pattern looks like that obtained with a spherical lens but the field decreases more smoothly as time increases. The field lasts longer than any of the axisymmetric cases because of the longer propagation times for the waves from the nonfocused dimension.

### III. WAVE PROPAGATION BOUNDARIES

Sometimes, knowing the location of the wave disturbance is useful, even without a calculation of the details of the wave front. It is shown in Appendix A that, for an axisymmetric case, the field can be obtained directly without transforms. The solution derived in Appendix A imposes the constraint that the field will exist only for those values of radial distance  $r$  that fall in the range

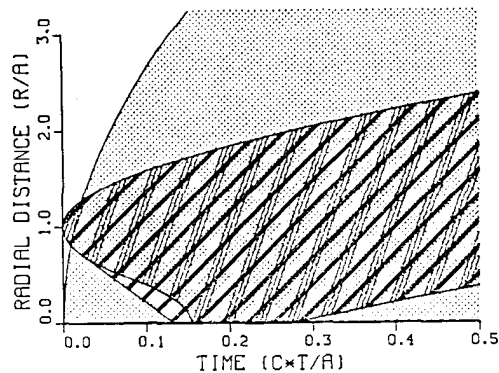


FIG. 13. Wave support at  $z = 5$  cm for a circular piston source (impulse excitation,  $A = 2.0$  cm,  $f = 10$  cm). (The single-dot region is for a spherical convex wave and the double-dot region is for a spherical concave wave. The solid-lined region is for a conical concave wave and the triple-lined region is for a parabolic concave wave.)

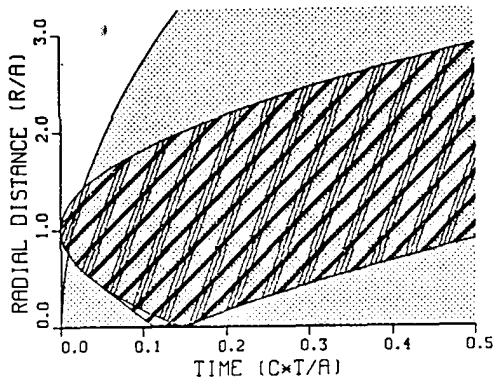


FIG. 14. Wave support at  $z = 10$  cm for a circular piston source (impulse excitation,  $A = 2.0$  cm,  $f = 10$  cm). (The single-dot region is for a spherical convex wave and the double-dot region is for a spherical concave wave. The solid-lined region is for a conical concave wave and the triple-lined region is for a parabolic concave wave.)

$$\min[(c^2\xi^2 - z^2)^{1/2} - r_i(t - \xi)] < r < \max[(c^2\xi^2 - z^2)^{1/2} + r_i(t - \xi)], \quad (21)$$

where the min and max operators and the variable  $\xi$  are discussed in Appendix A. This allowable range of values of  $r$  provides a simple way to "locate" the wave. In fact, it defines the edges of the wave envelope.

Figures 13–15 show the evolution of the wave domain at positions located distances of  $f/2$ ,  $f$ , and  $2f$ , respectively. On these plots the cross hatching indicates the extent of the wave. The light density dots represent the spherical convex wave; the double density dotted region is the spherical concave wave. The solid-lined region is the wave domain for the conical concave wave and the triple-lined region is for the parabolic concave wave. In all cases the spreading of the wave appears clearly, becoming wider when the observation point is further from the source. It is interesting to note that the parabolic wave and the spherical wave have the same wave domain. The conical wave has the same upper boundary as the former two cases, but the lower boundary is quite different. For the long-time behavior, all domains have the same lower boundary. For the  $f/2$  and  $2f$  locations, the field has an extended region of nonzero values on the propagation

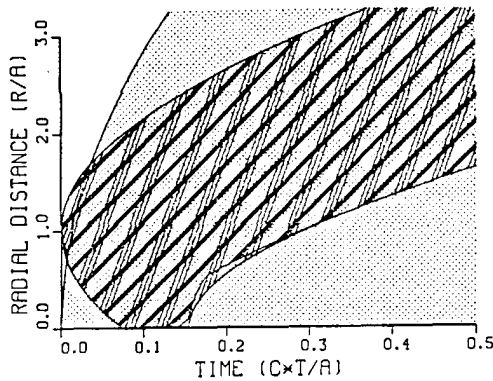


FIG. 15. Wave support at  $z = 20$  cm for a circular piston source (impulse excitation,  $A = 2.0$  cm,  $f = 10$  cm). (The single-dot region is for a spherical convex wave and the double-dot region is for a spherical concave wave. The solid-lined region is for a conical concave wave and the triple-lined region is for a parabolic concave wave.)

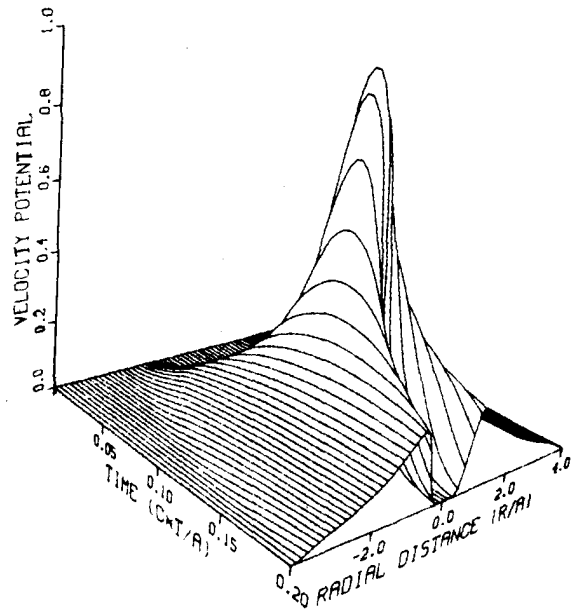


FIG. 16. Spherical concave wave with a circular cross section (pulse excitation,  $T = 0.04 A/c$ ,  $A = 2.0$  cm,  $f = 10$  cm,  $z = 10$  cm).

axis, whereas at  $z = f$  this region is reduced to a length that can be as small as a point (for a spherical lens).

#### IV. ARBITRARY TIME EXCITATION

For a time excitation different than  $\delta(t)$ , the diffracted wave is a convolution between the impulse response and the excitation function. Figures 16 and 17 show the result of two kinds of excitation on a spherical concave pattern observed at the focal point. The first excitation (Fig. 16) is a positive rectangular pulse with a duration of  $0.04 A/c$ , where  $A$  is lateral half-width of the input wave front. The smoothing effect of the time domain convolution is evident along the propagation axis. The signal lasts longer and the amplitude distribution is changed. The second excitation (Fig. 17) is a

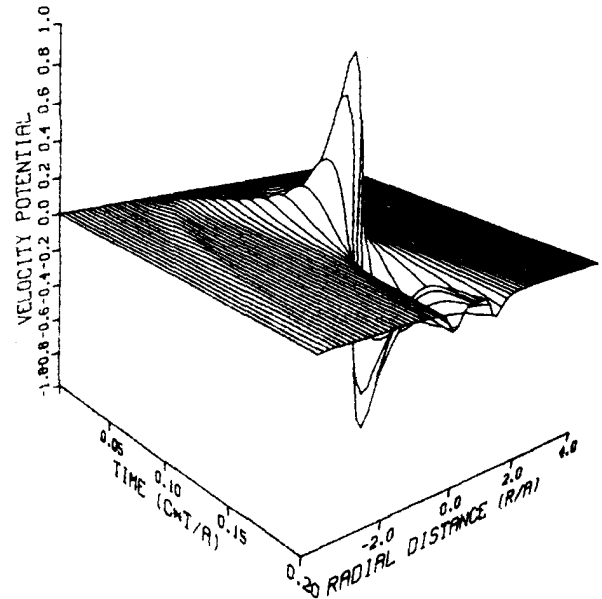


FIG. 17. Spherical concave wave with a circular cross section [resonant pulse excitation (i.e., one cycle of square wave),  $T = 0.04 A/c$ ,  $A = 2.0$  cm,  $f = 10$  cm,  $z = 10$  cm].

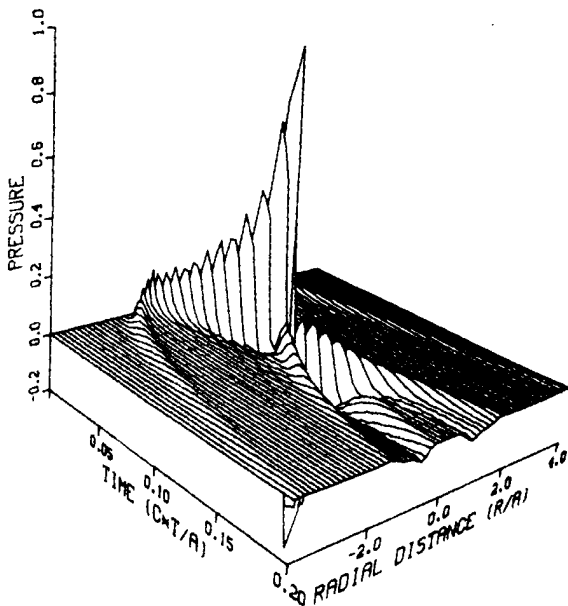


FIG. 18. Conical concave wave with a circular cross section (impulse excitation,  $A = 2.0$  cm,  $f = 10$  cm,  $z = 10$  cm).

resonant pulse (i.e., a one-cycle square wave) of the same overall duration. Here the differentiating effect of the opposite parts of the wave are evident but the peak observed with the impulse drive has been smoothed in this case.

### V. PRESSURE COMPUTATION

The pressure for an impulse temporal excitation can be obtained either by applying Eq. (18) in a straightforward manner or by differentiating the velocity potential obtained by using Eq. (16). The differentiation can be accomplished numerically by using existing numerical techniques or by convolving the velocity potential with the derivative of  $\delta(t)$  as approximated by two successive points with opposite sign. The latter method has been used to provide the pressure at the  $z = f$  plane for a conical wave as shown in Fig. 18. Consistent with this convolution, it is observed that the high temporal frequencies have been enhanced by this operation.

$$\phi(r, z, t) = \int_0^\infty \left( \int_b^t \sum_{i=1}^N \frac{s(\eta_i) J_0(\rho \eta_i) \eta_i J_0[\rho(c^2 \xi^2 - z^2)^{1/2}]}{|d'(x)|_{x=\eta_i}} d\xi \right) J_0(\rho r) \rho dp, \quad (A2)$$

where  $b$  is defined by

$$b = \max[z/c, t - \tau], \quad (A3)$$

with  $\max[a, b]$  being an operator that returns the larger of the arguments,  $\tau$  being the maximum delay of the curved wave front, and  $\eta_i$  is a variable given by

$$\eta_i = r_i(t - \xi). \quad (A4)$$

Inverting the integration order gives

$$\begin{aligned} \phi(r, z, t) &= \int_b^t \sum_{i=1}^N \frac{s(\eta_i) \eta_i}{|d'(x)|_{x=\eta_i}} \\ &\times \int_0^\infty J_0(\rho \eta_i) J_0[\rho(c^2 \xi^2 - z^2)^{1/2}] J_0(\rho r) \rho dp d\xi. \end{aligned} \quad (A5)$$

### VI. SUMMARY

A general approach for computing the radiated field of an arbitrary surface has been developed. Equations (16) and (20) give expressions for the fields. In most practical applications the expressions leading to the field simplify as can be seen in Appendix B, providing a useful tool for transducer design. For the important class of radially symmetric transducers, an expression for the radiated wave location in time and space may be developed using elementary expressions as in Eq. (21). The method does not require any specific sample interval in the time domain allowing a variable sampling interval as warranted. Once the impulse-excited response is known, it can be stored and the transient response for arbitrary time excitations can be computed by performing the time domain convolution. A 50-point convolution for all of the 64 spatial data points requires 1.4 s on an IBM 3033 computer.

### ACKNOWLEDGMENTS

This work was partially supported by the Foundation Research Program of the Naval Postgraduate School. Daniel Guyomar is a Research Associate of the National Research Council.

### APPENDIX A

In this Appendix an alternative form to Eq. (20) will be derived that produces an expression for the velocity potential that does not use any transform operations. A major secondary benefit of this derivation is an expression for the spatial domain of the wave that can be used for calculating the extent of the wave.

From Eq. (20) it follows that

$$\begin{aligned} \phi(r, z, t) &= B^{-1} \left[ \sum_{i=1}^N \frac{r_i^* s(r_i^*) J_0(\rho r_i^*)}{|d'(r)|_{r=r_i^*}} * J_0[\rho(c^2 t^2 - z^2)^{1/2}] \right]. \end{aligned} \quad (A1)$$

Expressing the convolution as an integral over  $\xi$  gives

The second integral is evaluated by the following identity<sup>18</sup>:

$$\begin{aligned} \int_0^\infty J_0(a\rho) J_0(b\rho) J_0(c\rho) \rho dp &= \frac{1}{2\pi} \left( \frac{1}{[a^2 - (b-c)^2]^{1/2} [(b+c)^2 - a^2]^{1/2}} \right) \\ \text{if } |b-c| < a < (b+c), & \\ = 0 \text{ otherwise.} & \end{aligned} \quad (A6)$$

Hence,

$$\begin{aligned} \int_0^\infty J_0(\rho \eta_i) J_0[\rho(c^2 \xi^2 - z^2)^{1/2}] J_0(\rho r) \rho dp &= \{ [r^2 - (\alpha - \eta_i)^2]^{1/2} [(\alpha + \eta_i)^2 - r^2]^{1/2} \}^{-1}, \end{aligned} \quad (A7)$$

where  $\alpha$  represents  $(c^2\xi^2 - z^2)^{1/2}$  and  $r$  must meet the condition

$$|\alpha - \eta_i| < r < \alpha + \eta_i. \quad (\text{A8})$$

Substituting the closed form solution in the previous expression yields

$$\begin{aligned} \phi(r, z, t) &= \sum_{i=1}^N \int_b^r \frac{s(\eta_i)\eta_i}{|d'(x)|_{x=\eta_i}} \\ &\times \{2\pi[r^2 - (\alpha - \eta_i)^2]^{1/2}[(\alpha + \eta_i)^2 - r^2]^{1/2}\}^{-1} d\xi, \end{aligned} \quad (\text{A9})$$

where

$$|\alpha - \eta_i| < r < \alpha + \eta_i. \quad (\text{A10})$$

This last constraint is very useful since it enables us to determine the domain where the wave will exist. It gives the wave location without any necessity for the calculation of the wave. The bounds of the domain are given by

$$r = \max(\alpha + \eta_i) \quad (\text{A11})$$

and

$$r = \min(|\alpha - \eta_i|), \quad (\text{A12})$$

where the max and min operators are now interpreted as returning the maximum and minimum values of the function of  $\xi$  in the argument where  $\xi$  ranges from  $b$  to  $t$ .

## APPENDIX B

This Appendix gives the relative displacement  $d(r)$  of the curved wave front, the zeros of  $ct - d(r)$ , and expressions for the derivative of  $d(r)$  with respect to  $r$ , evaluated at the zeros previously given. All of the relative displacements are given for the same depth  $d$  given by

$$d = f - (f^2 - a^2)^{1/2}, \quad (\text{B1})$$

where  $a$  is the depth of a concave lens focusing at a distance  $f$ .

### Spherical concave wave front

$$d(r) = (f^2 - r^2)^{1/2} - (f^2 - a^2)^{1/2}, \quad (\text{B2})$$

$$r_i = [a^2 - c^2t^2 - 2ct(f^2 - a^2)^{1/2}]^{1/2}, \quad (\text{B3})$$

$$|d'(r)|_{r=r_i} = \frac{[a^2 - c^2t^2 - 2ct(f^2 - a^2)^{1/2}]^{1/2}}{ct + (f^2 - a^2)^{1/2}}. \quad (\text{B4})$$

### Spherical convex wave front

$$d(r) = f - (f^2 - r^2)^{1/2}, \quad (\text{B5})$$

$$r_i = (2ctf - c^2t^2)^{1/2}, \quad (\text{B6})$$

$$|d'(r)|_{r=r_i} = (2ctf - c^2t^2)^{1/2} / (f - ct). \quad (\text{B7})$$

### Conical concave wave front

$$d(r) = \frac{-r[f - (f^2 - a^2)^{1/2}]}{a} + f - (f^2 - a^2)^{1/2}, \quad (\text{B8})$$

$$r_i = \frac{a[f - (f^2 - a^2)^{1/2} - ct]}{f - (f^2 - a^2)^{1/2}}, \quad (\text{B9})$$

$$|d'(r)|_{r=r_i} = [f - (f^2 - a^2)^{1/2}] / a. \quad (\text{B10})$$

### Parabolic concave wave front

$$d(r) = -\frac{r^2[f - (f^2 - a^2)^{1/2}]}{a^2} + f - (f^2 - a^2)^{1/2}, \quad (\text{B11})$$

$$r_i = a \left( \frac{f - (f^2 - a^2)^{1/2} - ct}{f - (f^2 - a^2)^{1/2}} \right)^{1/2}, \quad (\text{B12})$$

$$\begin{aligned} |d'(r)|_{r=r_i} &= (2/a) \{ [f - (f^2 - a^2)^{1/2}] \\ &\times [f - (f^2 - a^2)^{1/2} - ct] \}^{1/2}. \end{aligned} \quad (\text{B13})$$

### Square transducer with cylindrical lens

The following applies for a square transducer that is of length  $a$  on a side:

$$d(x_0, y_0) = [(f^2 - x_0^2)^{1/2} - (f^2 - a^2)^{1/2}] \pi (y_0/a), \quad (\text{B14})$$

$$x_{0i} = [a^2 - c^2t^2 - 2ct(f^2 - a^2)^{1/2}]^{1/2} \quad (\text{B15})$$

$$\begin{aligned} \left| \frac{\partial d(x_0, y_0)}{\partial x_0} \right|_{x_0=x_{0i}} &= \frac{[a^2 - c^2t^2 - 2ct(f^2 - a^2)^{1/2}]^{1/2}}{ct + (f^2 - a^2)^{1/2}}. \end{aligned} \quad (\text{B16})$$

Equation (8) simplifies in this case to

$$\begin{aligned} F_{xy} [s(x, y)\delta(ct - d(x, y))] &= [ct + (f^2 - a^2)^{1/2}] \frac{\sin f_y a}{f_y} \frac{\exp(-if_x x_{0i})}{x_{0i}}. \end{aligned} \quad (\text{B17})$$

- <sup>1</sup>F. Oberhettinger, "On transient solutions of the baffled piston problem," J. Res. Natl. Bur. Stand. **65B**, 1-6 (1961).
- <sup>2</sup>G. E. Tupholme, "Generation of acoustic pulses by baffled plane pistons," *Mathematika* **16**, 209-224 (1969).
- <sup>3</sup>P. R. Stepanishen, "Transient radiation from pistons in an infinite planar baffle," J. Acoust. Soc. Am. **49**, 1629-1637 (1971).
- <sup>4</sup>P. R. Stepanishen, "Experimental verification of the impulse response method to evaluate transient acoustic fields," J. Acoust. Soc. Am. **63**, 1610-1617 (1981).
- <sup>5</sup>G. R. Harris, "Review of transient field theory for a baffled planar piston," J. Acoust. Soc. Am. **70**, 10-20 (1981).
- <sup>6</sup>G. R. Harris, "Transient field of a baffled piston having an arbitrary vibration amplitude distribution," J. Acoust. Soc. Am. **70**, 186-204 (1981).
- <sup>7</sup>J. Weight and A. Hayman, "Observation of the propagation of very short ultrasonic pulses and their reflection by small targets," J. Acoust. Soc. Am. **63**, 396-404 (1978).
- <sup>8</sup>J. A. Archer-Hall, A. I. Bashter, and A. J. Hazelwood, "A means for computing the Kirchhoff surface integral for a disk radiator as a single integral with fixed limits," J. Acoust. Soc. Am. **65**, 1568-1570 (1979).
- <sup>9</sup>M. Fink, "Theoretical study of pulsed echocardiographic focusing procedures," in *Acoustical Imaging, Vol. 10*, edited by P. Alais and A. Metherell (Plenum, New York, 1980), pp. 437-453.
- <sup>10</sup>D. Guyomar and J. Powers, "Diffraction of pulsed ultrasonic waves in lossless and absorbing media" IEEE Trans. Sonics Ultrason. (submitted).
- <sup>11</sup>A. Penttinen and M. Luukkala, "The impulse response and pressure near-field of a curved ultrasonic radiator," J. Phys. D: Appl. Phys. **9**, 1547-1557 (1976).
- <sup>12</sup>M. Arditi, F. S. Foster, and J. W. Hunt, "Transient fields of concave annular arrays," *Ultrason. Imag.* **3**, 37-61 (1981).
- <sup>13</sup>D. R. Dietz, "Apodized conical focusing for ultrasonic imaging," IEEE Trans. Sonics Ultrason. **SU-29**(3), 128-138 (1982).
- <sup>14</sup>M. M. Goodstitt, E. L. Madsen, and J. A. Zagzebski, "Field patterns of pulsed, focused ultrasonic radiators in attenuating and nonattenuating media," J. Acoust. Soc. Am. **71**, 318-330 (1982).
- <sup>15</sup>W. N. Cobb, "Frequency domain method for the prediction of ultrasonic field patterns of pulsed, focused radiators," J. Acoust. Soc. Am. **75**, 72-80 (1984).
- <sup>16</sup>S. Candel, "An algorithm for the Fourier-Bessel Transform," *Comput. Phys. Commun.* **23**, 343-353 (1981).
- <sup>17</sup>M. S. Patterson and F. S. Foster, "Acoustic field of conical radiators," IEEE Trans. Sonics Ultrason. **SU-29**(2), 83-91 (1982).
- <sup>18</sup>A. Erdelyi, W. Magnus, F. Oberhettinger, and F. G. Tricomi, *Tables of Integral Transform, Vol. 2* (McGraw-Hill, New York, 1954), p. 52.